Machine Learning for Polaritonic Chemistry: Accessing Chemical Kinetics

N.B. When citing this work, cite the original published paper.

(article starts on next page)

Article

Machine Learning for Polaritonic Chemistry: Accessing Chemical Kinetics

Christian Schäfer,* Jakub Fojt, Eric Lindgren, and Paul Erhart*

Read Online

ACCESS | Metrics & More | Article Recommendations | SI Supporting Information

ABSTRACT: Altering chemical reactivity and material structure in confined optical environments is on the rise, and yet, a conclusive understanding of the microscopic mechanisms remains elusive. This originates mostly from the fact that accurately predicting vibrational and reactive dynamics for soluted ensembles of realistic molecules is no small endeavor, and adding (collective) strong light−matter interaction does not simplify matters. Here, we establish a framework based on a combination of machine learning (ML) models, trained using density-functional theory calculations and molecular dynamics to accelerate such simulations. We then apply this approach to evaluate strong coupling, changes in reaction rate constant, and their influence on enthalpy and entropy for the deprotection reaction of 1-phenyl-2-trimethylsilylacetylene, which has been studied previously both experimentally and using *ab initio* simulations. While we find qualitative agreement with critical experimental observations, especially with regard to the changes in kinetics, we also find differences in comparison with previous theoretical predictions. The features for which the ML-accelerated and *ab initio* simulations agree show the experimentally estimated kinetic behavior. Conflicting features indicate that a contribution of dynamic electronic polarization to the reaction process is more relevant than currently believed. Our work demonstrates the practical use of ML for polaritonic chemistry, discusses limitations of common approximations, and paves the way for a more holistic description of polaritonic chemistry.
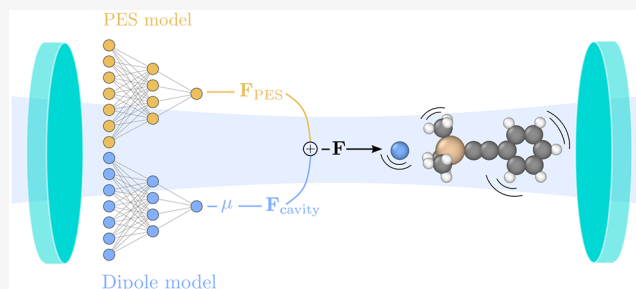
INTRODUCTION

If confined electromagnetic fields interact sufficiently strongly with matter, their excitations hybridize and give rise to new quasiparticles called polaritons.[1−6] Strong light−matter coupling has been used to alter chemical reactivity,[7−13] for which the term polaritonic chemistry has been coined. Vibrational strong coupling, in particular, is a promising candidate for practical application, demonstrating the inhibition,[9,14−16] steering,[17] and catalysis[18,19] of chemical processes at room temperature. Especially appealing features include the ability to nonintrusively control the path of the chemical reaction by adjusting external parameters, such as the distance between mirrors, and its existence in the absence of any externally provided energy. The latter sets polaritonics apart from Floquet engineering, which typically suffers from heating and uncontrolled dissipation processes.[20] Besides the specific control of chemical reactivity, polaritonics has been shown to give rise to a myriad of effects that range from commanding single molecules,[21−26] over altering energy transfer,[27−43] to the control of phase transitions in extended systems.[44−48]

Delivering a conclusive theoretical understanding for vibrational strong coupling has remained difficult. Especially, the experimentally observed resonance dependence in combination with an increase of rate changes for increasing emitter concentration and clear trends in chemical kinetics are

critical features that a theoretical model should capture. Initial attempts based on the standard transition-state theory[49−51] failed to reproduce any significant frequency dependence. Active development along the lines of Grote−Hynes[52−54] and Pollak−Grabert−Hänggi[55] theories showed some frequency dependence, but a connection to experiments has remained unsuccessful. A recent work by Schäfer et al.[13] tackled the problem from first-principles by utilizing quantum electrodynamical density-functional theory (QEDFT)[56−59] in combination with a self-consistent update of the nuclear motion according to Ehrenfest's equation for the experimentally investigated deprotection reaction of 1-phenyl-2-trimethylsilylacetylene (PTA).[14,15] This *ab initio* theory recovered critical components of the frequency dependence and suggested a microscopic theory based on adjusted vibrational energy redistribution for the cavity-induced modification of chemical reactivity. Chen et al. found experimental support for this

hypothesis using 2D spectroscopy.[10] Nonetheless, a prediction of kinetic quantities remained inaccessible, given the computational cost of QEDFT in combination with Ehrenfest dynamics.

In this work, we establish a framework that combines machine learning (ML) models, trained on data from density-functional theory (DFT) calculations, with molecular dynamics (MD) simulations to arrive at a more efficient, yet accurate description of the experimentally relevant S_N2 reaction of PTA[14] under strong coupling to a cavity. We find a pronounced frequency dependence for the chemical reaction rate constant along with changes in reaction enthalpy and entropy that are qualitatively consistent with the experiment. Interestingly, we discover frequency domains outside the experimentally validated window for which the present ML-accelerated approach predicts a rate constant enhancing character in contrast to earlier fully *ab initio* simulations,[13] which rather suggest inhibition. Here, we tentatively attribute this difference to the simplifications inherent to the present MD approach, suggesting that the latter, despite being widely used, has relevant limitations in its applicability to polaritonic chemistry. Further investigations beyond the scope of the present work will be needed to provide a more detailed understanding.

■ METHODOLOGY

Nonrelativistic quantum electrodynamics commonly starts at the minimal coupling Hamiltonian in the Coulomb gauge,[5,60−62] where all charged particles couple via longitudinal Coulomb interaction to each other and to the transverse vector potential ($\nabla \cdot \mathbf{A} = 0$)

$$\hat{H} = \sum_i^{N_e+N_n} \frac{1}{2m_i}(-i\hbar\nabla_i - q_i\hat{\mathbf{A}}(\mathbf{r}_i)/c)^2$$
$$+ \frac{1}{8\pi\varepsilon_0}\sum_{i,j}^{N_e+N_n}\frac{q_i q_j}{|\mathbf{r}_i - \mathbf{r}_j|}$$
$$+ \frac{\varepsilon_0}{2}\int d\mathbf{r}[\hat{\mathbf{E}}_\perp(\mathbf{r})^2 + c^2\hat{\mathbf{B}}(\mathbf{r})^2]$$

Polaritonic chemistry comes in different flavors that are distinguished by the frequency of the confined modes and the physical nature of the resonator, e.g., plasmonic, Fabry−Pérot, or whispering gallery cavities, which influences their fundamental coupling strength and quality factor. The accurate description of a realistic optical environment is a challenge in itself,[63−67] but simple single-mode models often suffice to obtain a qualitative understanding of the relevant emitter dynamics.

The goal of this work is to provide a qualitative investigation of vibrational strong coupling and its influence on chemical reactivity for experimentally relevant molecules. In particular, we focus on kinetic changes, their impact on enthalpy and entropy, and the consequences of simplifications in the MD. For this reason, we stay conceptually close to the previous work of Schäfer et al.[13] and rely on the Born−Oppenheimer approximation, projecting on the electronic ground-state and ignoring electronic polarizations induced by the cavity, such that the effective nuclear-photonic Hamiltonian takes the form[58,60,62,68]

$$\hat{H} = \hat{T}_{\text{nuclei}} + \hat{V}_{\text{PES}} + \hbar\omega_c\left(\hat{a}^\dagger\hat{a} + \frac{1}{2}\right)$$
$$- \sqrt{\frac{\hbar\omega_c}{2\varepsilon_0 V_c}}(\boldsymbol{\varepsilon}_c \cdot \hat{\boldsymbol{\mu}})(\hat{a}^\dagger + \hat{a}) + \frac{1}{2\varepsilon_0 V_c}(\boldsymbol{\varepsilon}_c \cdot \hat{\boldsymbol{\mu}})^2$$

The nuclei couple self-consistently to a single electromagnetic mode of the cavity, treated classically as the mode displacement $q_c(t) = \sqrt{\frac{\hbar}{2\omega_c}}\langle\hat{a}^\dagger + \hat{a}\rangle$ in the following, with frequency ω_c, effective cavity volume V_c, fixed polarization $\boldsymbol{\varepsilon}_c$, and molecular dipole moment $\hat{\boldsymbol{\mu}}$. Taking the classical limit for the nuclei, the system follows standard Hamiltonian mechanics with forces originating from the Poisson bracket $\{\mathbf{p}_j, \mathcal{H}\}$. In order to see appreciable changes for the dynamics of a single molecule, we choose large coupling values $g_0 = ea_0\sqrt{\omega_c/2\hbar\varepsilon_0 V_c}$ that are consistent with ref 13. We refer the interested reader to refs 13, 67, 69−71 for an extended discussion on the potential motivation of effective single-molecule coupling values. The chosen coupling is considerably larger than experimentally achievable values in Fabry−Pérot cavities, but the qualitative agreement with experiments suggests similar microscopic mechanisms. Our results and discussion can be partially transferred to plasmonic cavities which feature substantial single-molecule couplings.[21,23]

The *electronic* force acting on nucleus j is obtained from the potential energy surface (PES) according to

$$\mathbf{F}_{\text{PES}}^j = -\nabla_j V_{\text{PES}}(\mathbf{r}) \tag{1}$$

and contributes to the total force $\mathbf{F}^j = \mathbf{F}_{\text{PES}}^j + \mathbf{F}_c^j$ together with the *optical* force, which can be computed from the derivative of the dipole moment vector

$$\mathbf{F}_c^j = \frac{1}{\sqrt{\varepsilon_0 V_c}}\nabla_j[\boldsymbol{\varepsilon}_c \cdot \boldsymbol{\mu}]\left(\omega_c q_c(t) - \frac{1}{\sqrt{\varepsilon_0 V_c}}\boldsymbol{\varepsilon}_c \cdot \boldsymbol{\mu}\right) \tag{2}$$

The only interaction between light and matter arises then via the time evolution of the photonic mode $q_c(t)$ and the gradient of the projected dipole moment. The cavity mode displacement $q_c(t)$ depends on the history of the dipole moment (see Supporting Information Section IIA for details)

$$q_c(t) = q_c(0)\cos(\omega_c t) + \int_0^t \frac{\boldsymbol{\varepsilon}_c \cdot \boldsymbol{\mu}(t')}{\sqrt{\varepsilon_0 V_c}}\sin(\omega_c(t - t'))dt'$$

where vanishing of the initial momentum $\dot{q}_c(0) = 0$ is explicitly enforced.

We leverage the modular character of the forces by implementing a custom ("cavity") propagator using the ASE Python package.[72] The calculator requires merely the initial molecular configuration as well as estimators for the forces arising from the PES (eq 1) and the dipole moment vector (eq 2). Possible estimators may include machine-learned models, empirical force fields, and even *ab initio* calculations based on, e.g., DFT. We note that this approach can also be easily combined with the embedding radiation-reaction approach[67] in the future, thus providing an elegant path for including collective coupling and realistic optical environments.

Obtaining forces and dipole derivatives, thus, represents the main obstacle in the MD approach, as in reality, a molecule can easily pass through tens of thousands of configurations before a
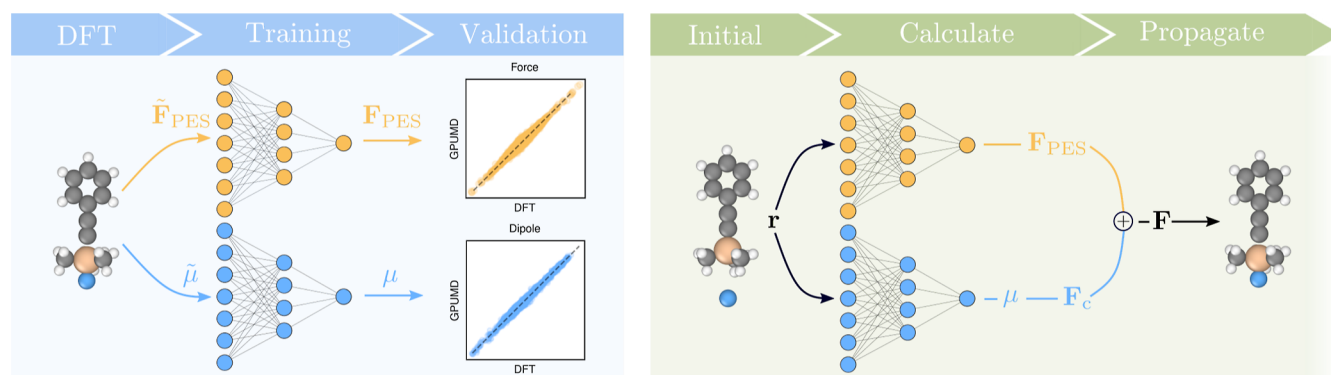
Figure 1. Methodological flow chart. DFT is used to calculate energies, forces, and dipoles. Positional information of a structure is translated into descriptor space, and NEP models for the PES and the dipole moment vector μ are trained using supervised learning (left-hand side). The final models are combined to compute the effective forces acting on the nuclei that are then used to propagate the system in time (right-hand side).

reaction occurs. One possible, but practically often too expensive, approach is to perform *ab initio* electronic structure calculations at each point, usually referred to as *ab initio* MD.[73] While the cost of a single DFT calculation might be comparably low, the sheer quantity of calculations required for a statistically meaningful evaluation, i.e., obtaining thousands of trajectories with tens of thousands of DFT evaluations each, is highly prohibitive and practically limits the simulation time as well as the system and ensemble size. Another prominent approach is based on empirical force fields,[74,75] which are computationally orders of magnitude more efficient than DFT calculations. They are, however, restricted with respect to accuracy as well as availability and offer limited transferability. Even if we would have a suitable force field for a system, there is no guarantee that, e.g., a force field fitted in an aqueous solution will perform well for simulations in vacuum and vice versa.

As we will show in the following, employing ML techniques in combination with MD provides a feasible, predictive, and scalable path, striking a balance between computational cost and accuracy.

Electronic and Optical Forces Using Neural Networks. In the present work, we developed two different models using the neuroevolution potential (NEP) framework as implemented in the GPUMD package.[76−78] One for predicting the PES $V_{PES}(\mathbf{r})$, as well as the associated force $\mathbf{F}_{PES}(\mathbf{r})$, and another for predicting dipole moments $\mu(\mathbf{r})$ (Figure 1; left). We refer the reader to Supporting Information for an extensive discussion of the training and testing procedures of both models.

The NEP models are then combined to obtain the total force used to propagate the system in time with a custom integrator implemented in the ASE package[72] (Figure 1; right). We refer the interested reader to refs 78 and 79 for a more extensive presentation of the NEP framework and its application to tensorial quantities.

The NEP approach employs a simple forward bias multilayer perceptron with a single hidden layer in combination with a flexible descriptor to predict the atomic energy U_i for each atom in a system by decomposing the total energy into individual contributions from each atom, $U = \sum_i U_i$. The model consists of a fully connected network with a single hidden layer, yielding the following expression for the predicted energy

$$U_i = \sum_{\mu=1}^{N_{neu}} w_\mu^{(1)} \tanh\left(\sum_{\nu=1}^{N_{des}} w_{\mu\nu}^{(0)} q_\nu^i - b_\mu^{(0)}\right) - b^{(1)} \tag{3}$$

The two weight matrices $w_{\mu\nu}^{(0)}$ and $w_\mu^{(1)}$ are the weights for the input and hidden layers, with $b_\mu^{(0)}$ and $b^{(1)}$ being their respective biases, and tanh is used as the activation function for the input layer. The so-called descriptor vector q_ν^i of length N_{des} indexed by ν can be seen as a representation of the local chemical environment of atom i, is a function of the pairwise distances $\mathbf{r}_{ij} = \mathbf{r}_i - \mathbf{r}_j$, and serves as an input to the network. If q_ν^i uniquely describes a molecular configuration is determined by a basis expansion over N-body interactions within a cutoff radius r_c. The expansion is truncated at 4-body interactions, which is sufficient to accurately describe local changes. A key feature of the NEP formalism is that these descriptors also contain trainable parameters, which allows the network to tailor the descriptors more individually to different atomic configurations. Predictions for forces and virials can be obtained by computing the gradient of the predicted site energies, i.e., the PES force acting on atom i is

$$\mathbf{F}_i = \sum_{i \neq j} \frac{\partial U_i}{\partial \mathbf{r}_{ij}} - \frac{\partial U_j}{\partial \mathbf{r}_{ji}} \tag{4}$$

Additionally, the NEP formalism may be extended to predict other tensorial properties, such as dipole moments, which are obtained as

$$\mu = -\sum_i^N \sum_{j \neq i} \mathbf{r}_{ij} \cdot \left(\mathbf{r}_{ij} \otimes \frac{\partial U_i}{\partial \mathbf{r}_{ij}} \right)$$

$$= -\sum_i \sum_{j \neq i} r_{ij}^2 \left(\frac{\partial U_i}{\partial \mathbf{r}_{ij}} \right) \tag{5}$$

Having replaced the estimates for forces and dipoles with our NEP models, we are now equipped to address the question of how an optical resonator might influence the S_N2 reaction.

RESULTS AND DISCUSSION

In a first step, we perform ensemble calculations with preserved particle number, volume, and temperature (NVT) in the absence of the cavity to obtain a reference value for the transition-state enthalpy of $\Delta H^{\ddagger} = 0.345$ eV $= 33.3$ kJ mol^{-1}. The latter is in excellent agreement with experimental
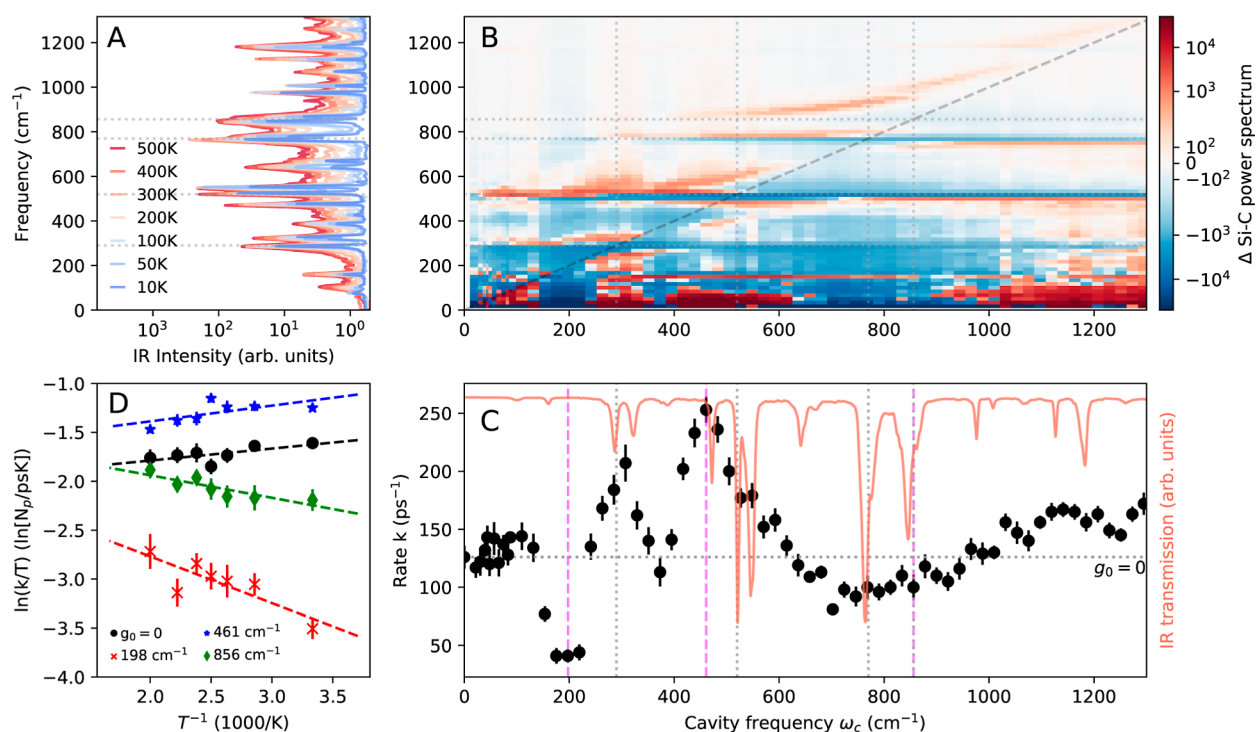
Figure 2. Modification of reaction rate constants by coupling to the cavity. (A) Temperature-dependent infrared spectrum outside the cavity, projected on the cavity polarization. (B) Difference in power spectra of the Si−C bond for PTAF$^-$ coupled to the cavity with g_0/ω_c = 1.132 at 400 K vs the same system outside the cavity. Gray-dotted lines ($\hbar\omega$ = 290, 520, 770, 856 cm^{-1}) serve as guides to the eye. (C) Rate constant (black dots) and standard error (black bars) for the unidirectional reaction PTAF$^-$ → FtMeSi + PA$^-$ at 400 K and g_0/ω_c = 1.132. The rate constant is calculated as number of products after 2 ps. Transmission spectrum at 400 K (red line, defined as negative of absorption spectrum). Vertical magenta-colored-dashed lines indicate relevant frequencies used for the kinetic estimates in (D). (D) Eyring plot in free space and for relevant cavity resonances given in inverse centimeter with g_0/ω_c = 1.132. The extracted change in enthalpy and entropy is collected in Table 1. Negative enthalpy originates from the selected initial state and should only be interpreted relative to the equilibrium enthalpy (see text). The rate constant is calculated as number of products N_p per ps.

estimates of $\Delta H^\ddagger$ = 35 ± 4 kJ mol^{-1}.[15] DFT calculations using the nudged elastic band approach in combination with a transition-state optimization provide a higher barrier of 0.43 eV. This illustrates the limitation of estimating the enthalpy from the 0 K energy difference between minimum and transition states and the significance of vibrational contributions. Detailed information as well as various benchmarks can be found in Supporting Information. We define a reaction event when the relevant Si−C bond is stretched beyond 3.5 Å, which exceeds the transition-state Si−C distance of approximately 3 Å, to avoid counting eventual recrossing events. If not further specified, all observables are obtained from ensemble averages involving 1000 trajectories. They are initialized with Boltzmann sampled velocities (kept fixed when changing cavity parameters) at the nonequilibrium F$^-$ + PTA state used in ref 13 and propagated preserving particle number, volume, and energy (NVE). The cavity displacement is selected such that no electric field exists at time zero; i.e., the cavity force is zero. The initial state features an energy difference to the minimum PTAF$^-$ configuration of 1.34 eV. This shortens the necessary calculation time and avoids spurious interplay between thermostat and cavity. One should note that it also limits the transferability of the obtained rate constants to experimental observations. Nonetheless, we can extract changes in the rate constant and thus contribute valuable insight into the current hypothesis behind polaritonic chemistry.

Strong Coupling. Strong coupling requires the existence of optically active vibrational modes near the cavity frequency. Certainly, the vibrational spectrum is sensitive to temperature, as illustrated in Figure 2A. The reaction-defining Si−C bond contributes fractionally to most vibrational excitations but primarily at frequencies below 1300 cm^{-1}. Figure 2B illustrates the corresponding power spectrum during the reaction process at 400 K with strong coupling to the cavity. We keep the ratio g_0/ω_c constant in our calculations. Changing the cavity length L_c ($V_c = A_c L_c$), which is the experimental way to tune the frequency of the Fabry−Pérot cavity, leads in a simplified mode picture to $g_0 \propto \sqrt{\omega_c}/\sqrt{L_c}$ and $\omega_c \propto 1/L_c$, i.e., a larger distance between the mirrors reduces both frequency and coupling strength with $1/L_c$. Following the gray-dashed diagonal $\omega = \omega_c$, we can clearly identify multiple avoided crossings (hybridizations) with substantial Si−C contribution. Each of the avoided crossings contributes with additional low-energy components (following the vertical gray-dotted lines), suggesting comparably slow changes, i.e., on the time scale of the reaction. The reorganization of the methyl groups and proper F−Si−C alignment (bending modes) are critical steps in the reaction pathway. Their interplay with the cavity manifests in the constant contribution at $\hbar\omega \approx 117$ cm^{-1}, which is further detailed near the end of the manuscript.

Resonance Dependence. Intuitively, we expect the low-frequency Si−C contribution to play a major role in the reactivity, as the defining Si−C bond-breaking step requires a few hundred femto seconds. Given the fact that the

contribution changes nonmonotonically, it is not surprising that the rate constant also changes nonmonotonically (Figure 2C). We observe pronounced regions of inhibited reactivity, especially around 200 cm^{-1} and the domain including the 770 and 856 cm^{-1} vibrations. Furthermore, a near 2-fold enhancement of the rate constant at around 290 and 460 cm^{-1} is visible. Experimental investigations are available only near 856 cm^{-1} and support the general inhibiting trend in this domain, albeit featuring an inhibiting effect only in a narrow frequency window. A nonmonotonous rate change, however, is in conflict with previous *ab initio* simulations in ref 13. Interestingly, the most pronounced feature at 200 cm^{-1} seems to be not related to any optical excitation and is also not connected to the curvature at the transition state, which we estimate with both our NEP model and DFT calculations to be approximately 73 cm^{-1}.

We will elaborate the conceptual differences to ref 13 and possible explanations later, but it should be noted that a strict comparison is difficult due to the difference in observable, temperature, and a substantial difference in statistical sampling. The slow but steady increase in the rate constant for large frequencies could partially originate from numerical deviations in the finite-difference approximation of the dipole gradient (see conservation of energy in Supporting Information). With this in mind, let us disentangle the mechanism behind the catalyzing and inhibiting effects by estimating enthalpic and entropic changes.

Kinetics. We repeat calculations for the rate constant for various temperatures at four frequencies extracted from Figure 2C that are characteristic for their respective frequency domains. The results are collected in an Eyring plot (Figure 2D) and indicate conceptually different mechanisms for inhibition and rate constant enhancement. The corresponding Arrhenius plot is provided in Supporting Information. We would like to emphasize that those changes originate from the independent dynamics of an ensemble of trajectories and the Eyring equation

$$k = \kappa \frac{k_B T}{h} e^{\Delta S^{\ddagger}/k_B} e^{-\Delta H^{\ddagger}/k_B T}$$

is used only to enable a comparison with the experimentally extracted enthalpy and entropy. Changes in transmission coefficient κ thus contribute to an altered entropy.

Without a cavity environment ($\omega_c = 0$, black), we estimate a weak but negative enthalpic barrier ΔH. This should be seen as the change induced by the chosen initial state and *NVE* conditions, i.e., the elevated initial state will provide almost no energetic barrier, and yet, the cavity will alter this "barrier". We demonstrate in Supporting Information Section IIB that performing rate constant estimates under *NVT* conditions and sufficient equilibration time provides accurate rates in agreement with the experiment outside the cavity, i.e., our methodology provides the correct kinetics outside the cavity, but the chosen initial state shifts the enthalpy up in energy. We collect the changes in enthalpy $\Delta\Delta H$ and entropy $\Delta\Delta S$ in relation to the cavity-free *NVE* results in Table 1.

At the inhibiting frequencies of 198 cm^{-1} (red) and 856 cm^{-1} (green), the enthalpy ΔH increases considerably. The $\omega_c = 198$ cm^{-1} excitation, without optically active vibrational mode support, shows a weak increase in entropy, suggesting that the dynamic effect of the cavity is to "simply" raise the transition-state barrier. Even though $\omega_c = 856$ cm^{-1} (green) shows an overall smaller change, entropic changes are large

Table 1. Change in Enthalpy and Entropy Compared to Free-Space Eyring Result (Black Data in Figure 2D)

ω_c (cm^{-1})	$\Delta\Delta H$ (eV)	$\Delta\Delta S$ (k_B)
198	+0.052	+0.22
461	−0.003	+0.32
856	+0.030	+0.56

compared to the other frequencies, which suggests that the cavity assigns a slightly stronger dissociative character to the reaction. Both features are in qualitative agreement with experiment.[14,15] Taking into account that the correct enthalpy obtained from our *NVT* calculations in free space is $\Delta H^{\ddagger} = 0.345$ eV, the inhibiting frequencies render the reaction more temperature sensitive, which can lead to enhanced rates for large temperatures. Such a trend in temperature sensitivity has been widely observed in experiments.[14,15,18]

At the catalyzing frequency $\omega_c = 461$ cm^{-1}, on the other hand, there is almost no change in enthalpy, but there is a noticeable change in entropy, suggesting that the mechanism dominating here is not related to the experiments which typically showed a clear change in enthalpy. It is important to emphasize that utilization of the Eyring equation is especially problematic in this domain as a further increase in reaction speed implies that the trajectory will spend less time around the reactant well. This in turn implies that the kinetic arguments underlying the Eyring equation, i.e., a separation of time scales between reactant equilibration and transmission process, become questionable since the transition state is then part of the equilibration process. Nonetheless, a similar offset in the rate constant without change in enthalpy has been observed when employing Grote−Hynes rate theory.[80] All three domains relate to different kinetic changes and, thus, suggest slightly different mechanisms.

Vibrational Dynamics. Let us shine a bit more light on the mechanistic differences between the chosen frequency domains that catalyze (461 cm^{-1}) or inhibit reactions without (198 cm^{-1}) or with (856 cm^{-1}) vibrational support. Figure 3 illustrates the accumulated difference in normal-mode occupation between a given cavity frequency and free space during the reaction averaged over the full ensemble. The corresponding occupation differences are presented in the Supporting Information, where the overall structure for $\omega_c = 856$ cm^{-1} is comparable to ref 13. Optically relevant domains around 300, 550, 770, and 1200 cm^{-1} are noticeably affected more strongly when selecting cavity frequencies $\omega_c = 461$ cm^{-1} and $\omega_c = 856$ cm^{-1}. Choosing a specific cavity frequency affects the vibrational modes in energetic proximity more strongly. This effect is especially apparent for $\omega_c = 856$ cm^{-1} which involves the C=C stretching mode around 1200 cm^{-1} (see the green bars in Figure 3). We quantify the changes in cross-correlation between the IR spectrum and the accumulated (absolute) difference [Figure 3 top (bottom)] in Table 2 with the help of the relative difference between the cross-correlation for $\omega_c \in \{198, 461, 856\}$ cm^{-1} and the high-frequency value $\omega_c = 1251$ cm^{-1}. The resulting change indicates how strongly differences in the normal-mode occupation correlate with infrared activity. Changes in the normal-mode occupation for cavity frequencies with optical support, i.e., $\omega_c = 461$ cm^{-1} and $\omega_c = 856$ cm^{-1}, feature a larger correlation.

Overall stronger correlation for $\omega_c = 461$ and 856 cm^{-1} suggests that the microscopic mechanism is more strongly characterized by redistribution of vibrational energy between
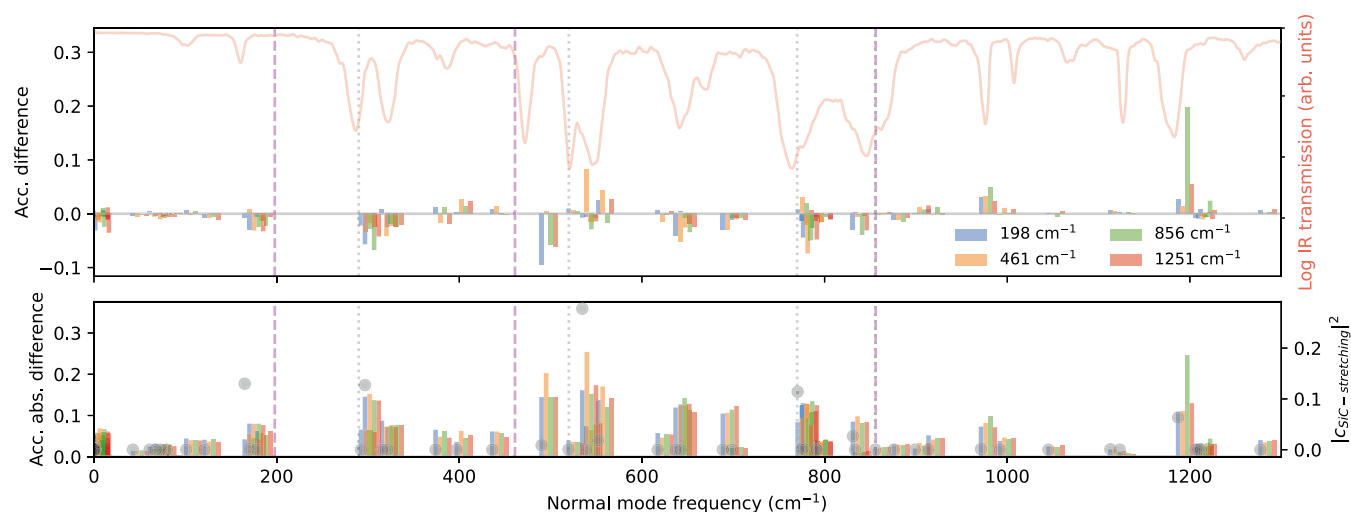
Figure 3. Change in mode occupation due to coupling to the cavity. Accumulated (top) and accumulated absolute (bottom) difference in the normal-mode occupation for different cavity frequencies (given in cm^{-1}) with $g_0/\omega_c = 1.132$ vs free space at 400 K. The corresponding differences in occupation and numerical details are presented in the Supporting Information. We quantify the relative changes in cross-correlation between the IR spectrum and the accumulated (absolute) difference in Table 2. Gray circles show the contribution of Si−C stretching to the vibrational normal mode (see text and Supporting Information Section IIF). Note that we average here over a time domain of 2 ps and not 0.7 ps as in ref 13.

Table 2. Relative Difference of the Cross-Correlation Function $\delta\delta C_{\omega_c}^{A(A)D} = \delta C_{\omega_c}^{A(A)D}/\delta C_{1251}^{A(A)D} - 1$[a]

ω_c (cm^{-1})	$\delta\delta C_{\omega c}^{AD}$ (%)	$\delta\delta C_{\omega c}^{AAD}$ (%)
198	+0.24	+1.09
461	+66.3	+11.3
856	+45.3	+3.11

[a]Only the frequency domain illustrated in Figure 3 was utilized in the calculation of the cross-correlation function. We define $\delta C_{\omega_c} = \sum_i |IR(\omega_i)\cdot A(A)D_{\omega_c}(\omega_i)|/\sum_iIR(\omega_i)$, where $A(A)D$ represents the accumulated (absolute) difference

optically active modes and is thus optically mediated, as suggested in ref 13. In other words, the cavity facilitates energy exchange between optically active modes, especially within an energy window around the cavity frequency. Since the Si−C bond is an essential ingredient in the reaction process, a stronger involvement of the Si−C bond stretching (gray circles shown in Figure 3) in the affected normal modes will result in a larger impact on the chemical reaction. Then also, the vibrational analysis supports the previous hypothesis that chemical changes without support by optically active modes follow, to a certain degree, a different mechanism.[13] Surprisingly, however, even though ω_c = 461 and 856 cm^{-1} seem to share a very similar mechanism based on the ML + MD analysis, their effect on the enthalpy is qualitatively different (catalyzing vs inhibiting). Albeit previous *ab initio* calculations did not provide access to kinetic changes, the corresponding analysis provided no indication of a qualitative difference between ω_c = 461 cm^{-1} and ω_c = 856 cm^{-1}.[13] Let us reflect in the following section on the underlying approximation of our MD simulations in order to understand this contradicting observation.

Limitations of Simplified Cavity MD. The experimentally relevant domain around 856 cm^{-1}[14,15] is inhibited in our ML + MD calculations as well as in experiment and the recent *ab initio* QEDFT calculations with nuclear motion according to the Ehrenfest equations of motion.[13] The existing information on changes in chemical rates is thus consistent at ω_c = 856

cm^{-1}. On the other hand, the ML + MD calculations show enhanced rate constants at 461 cm^{-1}, an effect that has not been observed in the QEDFT calculations. A direct comparison of Figure 2 to ref 13 is, however, problematic since the latter used an incomplete sampling with a strong bias toward the high-energy tail of the Boltzmann distribution. In other words, the QEDFT results were obtained at an effectively higher temperature.

To allow for a more reliable comparison and to shed light on the apparent discrepancy between the approaches, we recalculated the rate constant changes with our ML + MD approach for the same initial velocities as the QEDFT calculations. Figure 4 sets the newly obtained rate constants from our ML + MD calculations (black dots) in contrast with the average Si−C distances calculated with QEDFT (blue stars) and taken from ref 13. We demonstrate in Supporting Information Section IID that the Si−C distance and the rate constant are well correlated in this case.

Ignoring the offset, a slight frequency shift, and the qualitatively different behavior near ω_c = 0, the overall shapes of the reaction rate constant profiles shown in Figure 4 are consistent. Given identical initial conditions, ML + MD and QEDFT provide thus a similar *profile* in the intermediate frequency domain, but this profile is elevated into the catalyzing domain for the ML + MD calculations. Looking back at Figure 2C, the major catalyzing feature of the ML + MD calculations at 461 cm^{-1} is consistent between proper (Figure 2C) and incomplete sampling (Figure 4). Especially low-frequency features are considerably shifted and altered in strength, potentially originating from the quicker average reaction time when sampling from the high-energy tail of the Boltzmann distribution, which implies that the cavity has less time to influence the reaction. We recall that shorter reaction times emphasize dynamic contributions, calling the concept of a kinetic reaction rate further into question. It is thus plausible that the overwhelming catalyzing strength is partially an artifact, and we therefore suggest to focus on the qualitative trend only. This leaves but one question: Can we draw any
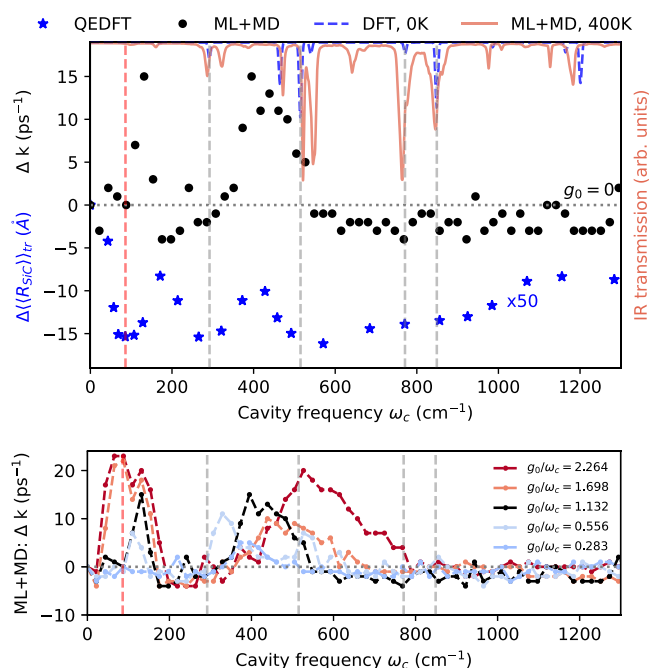
Figure 4. Impact of dynamic electronic polarization. (Top) Black dots: change in the rate constant compared to free space for the unidirectional reaction PTAF$^-$ → FtMeSi + PA$^-$ using the 30 initial configurations used in ref 13 and g_0/ω_c = 1.132, but propagated with our NEP-based MD calculator. Blue stars: change in the average Si−C distance obtained from the QEDFT calculations in ref 13 amplified by a factor 50. Transmission spectrum obtained from DFT at 0 K with harmonic approximation consistent with ref 13 (blue dashed) and using our NEP model and GPUMD at 400 K *NVE* conditions (red solid). Vertical lines indicate characteristic features observed in ref 13. We show in Supporting Information Section IID that the Si−C distance and the rate constant are clearly correlated, i.e., the qualitative trend of QEDFT and ML + MD can be set in relation. (Bottom) ML + MD calculations repeated for different fundamental light−matter coupling strength.

conclusion about the mechanism of vibrational strong coupling from the observed discrepancy?

Relevance of Dynamic Electronic Polarization. As we established at the beginning, effective nuclear forces comprise the adiabatic electronic Born−Oppenheimer forces and the dynamic optical forces mediated via dipolar changes induced by nuclear displacement. This implies that the static polarization of the electric system due to the instantaneous cavity field as well as its nonadiabatic corrections, quantum nuclear, and quantum light−matter effects is absent, as is the case in most available theoretical investigations for chemical reactivity affected by strong coupling. Nonadiabatic electron−nuclear effects are expected to play a minor role as the electronic excited space is separated by about 3 eV at minimum and transition states. While there has been recent discussions about the potential need to consider the full quantum light−matter interaction in model systems to recover resonant features in the cavity modified reactivity,[81,82] it remains up to debate if this is true for realistic systems under standard ambient conditions. Such a question requires a nuanced discussion based on the specific system at hand, and we expect that the answer will vary strongly between collective and single molecular coupling.

Lastly, and probably most importantly, nuclear motion will induce strong optical fields, which in turn polarize the electronic system. This happens similar to a static external potential $\propto g_0 q_c \boldsymbol{\varepsilon}_c \cdot \hat{\boldsymbol{\mu}}_e$ or via the self-polarization contributions $g_0^2/\omega_c(\boldsymbol{\varepsilon}_c \cdot \boldsymbol{\mu}_n)(\boldsymbol{\varepsilon}_c \cdot \hat{\boldsymbol{\mu}}_e)$ (and $g_0^2/(2\omega_c)(\boldsymbol{\varepsilon}_c \cdot \hat{\boldsymbol{\mu}}_e)^2$). It is important to note that this polarization, although being instantaneous in the sense of the Born−Oppenheimer approximation, is inherently *dynamic* due to its origin from nuclear dynamics. We will label this effect in the following *dynamic* electronic polarization to emphasize that the effect does not originate from the hybridization of the light−matter ground state nor from electronic transitions (nonadiabatic coupling elements). This form of dynamic electronic polarization can be formally incorporated via the cavity Born−Oppenheimer approximation,[83,84] where the photonic displacement q_c is considered as an additional parametric variable and self-polarization contributions are added to the electronic structure calculations. When included, the dynamic electronic polarization can lead to notable asymmetries in the vibrational polaritons[13,84] and increase the effective reaction barrier, thus reducing the chemical reactivity.[71,85] Our current ML + MD calculations are lacking the possibility to describe this dynamic electronic polarization and will thus tend toward a higher reactivity and more symmetric Rabi splittings (see Figure 2B).

Consulting perturbation theory, the cavity induced changes in the electronic ground-state energy scale approximately as $\propto g_0^2/\omega_c[1 - \omega_c/(\Delta E_e + \omega_c)]$,[59,86] where $\Delta E_e \gg \omega_c$ represents the electronic excitation energy for the dominant dipole transitions. Perturbation theory should provide an adequate estimate for electronic changes since the expansion parameter $\propto 1/\sqrt{V_c}$ is small and only g_0/ω_c takes appreciable values. Fixing again g_0/ω_c = const. and noticing a larger dipole near the transition state (see Note[a]), an additional increase of the barrier $\propto \omega_c$ would be missing in our MD calculations compared to the QEDFT calculations. As a result, our ML + MD calculations provide sensible values near $\omega_c = 0$ and for large frequencies but have the tendency to be overly reactive in the intermediate domain as they lack an additional suppression from dynamic electronic polarization.

Larger cavity frequencies ω_c are driven resonantly only by vibrational modes of comparable frequency. If such a vibration contributes to the reaction, i.e., whether it will be noticeably excited during the reaction, depends largely on its Si−C contribution. If the cavity can exert notable effects on a reaction event will therefore depend on three time scales: (i) the strongly occupied reactive modes of frequency ω_{SiC}, (ii) the cavity frequency ω_c, and (iii) the frequency with which the PES is modulated ω_{modPES} (dynamic electronic polarization) as consequence of the nuclear dynamics. Since ω_{modPES} depends partially on the optical mode q_c, which oscillates with ω_c, it seems intuitive that the largest effect of dynamic electronic polarization on the reactive modes ω_{SiC} can be expected when all time scales are comparable. As emphasized by Figures 2B and 3, most of the optically active modes with relevant Si−C contributions are located below 840 cm^{-1}. The *dynamic* contribution of electronic polarization then plays a decreasing role at higher frequencies. How the precise interplay between nuclear motion, strongly coupled cavity, and cavity-modulated electronic polarization affects the reactivity goes beyond the scope of this work. Our results emphasize the role of dynamic electronic polarization but also indicate that it is unlikely to be the only relevant contribution. Ample experimental work, however, demonstrated changes in solute−solvent interaction[18,88] under vibrational strong coupling, which indicates the

involvement of dispersive interactions mediated by electronic polarization.

Additional Considerations. Let us consider the analogy of our MD calculations as the self-consistently driven dynamic of a ball on a high-dimensional energy surface. If we intend to cross a specific barrier but let the cavity periodically remove kinetic energy before inserting it back at a later time, we can imagine that the likelihood to cross the barrier is modulated by the frequency with which the cavity is oscillating. We can indeed observe such an effect at low cavity frequencies, where reaction events appear in bursts that are related to the cavity frequency. Figure 5 shows the Fourier transform of the
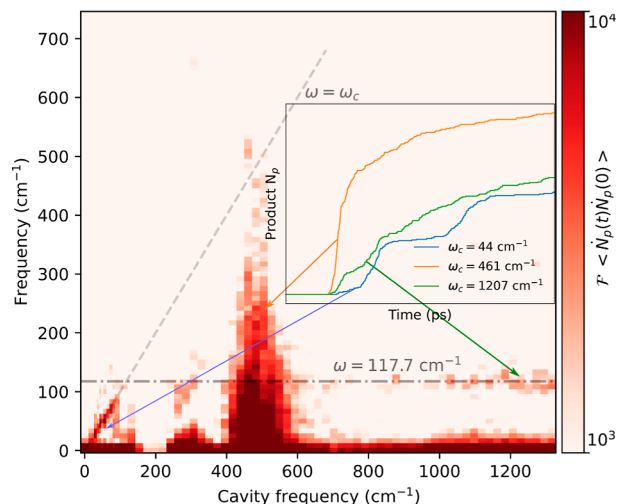

Figure 5. Frequency dependence of reaction bursts. Fourier transform of the autocorrelation function of changes in the number of products $|\mathcal{F}\langle\dot{N}_p(t)\dot{N}_p(0)\rangle|$ at 400 K and $g_0/\omega_c = 1.132$, where N_p is the number of products. The inset shows the time-dependent accumulation of products at low frequencies, in the strongly catalyzing domain, and at high cavity frequencies where the 117 cm^{-1} mode attains a pronounced role during the reaction (see text).

autocorrelation function of the change in product of the S_N2 reaction. The linear dispersion at low frequencies clearly shows that the bursts in reaction events are correlated with the cavity frequency, a feature that is absent in the QEDFT calculations of ref 13. This trend continues up to a bending mode at 117 cm^{-1}, which contributes to the necessary rearrangement of the methyl groups. Bending modes have recently been identified as a relevant component in the cavity-enhanced charge transfer,[38] which might suggest that the observed interplay between linear dispersion and bending mode could be of wider relevance. Surely, this simplified picture of modulated reactivity can only hold if vibrational energy redistribution into other modes is unlikely, a condition that is rarely fulfilled and explains why the effect disappears quickly.

It seems intuitive to assume that the here-observed discrepancy, supposedly scaling with g_0^2, should only matter for sizable coupling strengths, and the change in the rate constant should approach the cavity-free reference value monotonously for decreasing coupling. However, this would either imply that the ML + MD calculation would need to qualitatively change from catalysis to inhibition while approaching $k_{g_0=0}$, which is not observed in Figure 4 (bottom), or that the QEDFT calculations should become catalyzing during this process, for which there was no indication in ref 13.

One might thus draw the conclusion that dynamic electronic polarization, missing in ML + MD, is required for the qualitative prediction of chemical changes via single-molecule vibrational strong coupling at most frequencies and for all coupling values. Furthermore, such features might even play a role in collectively coupled systems where individual molecules can exhibit large dynamic electronic polarization in response to collective vibrational dynamics.[70,71]

Supporting Information Section IIH includes the same investigation performed in this section using a second NEP model based on DFT data calculated with a smaller electronic basis-set. The overall trend up to 700 fs (as in ref 13) is consistent with the here-presented ML + MD calculations. Since both ML + MD investigations show a consistent qualitative deviation from the QEDFT calculations, they both support the argument of dynamic electronic polarization. In addition, the smaller basis-set results in a smaller reaction barrier, which reduces the significance of the catalyzed trajectories at longer times. The most characteristic feature remaining after 2 ps is a strong inhibition around 200 cm^{-1}, which is consistent with Figure 2C. This emphasizes that estimates of kinetic quantities require sufficient sampling.

Sampling, calculating, and learning potentials for every frequency and coupling, in order to obtain the full cavity Born–Oppenheimer surface, is in principle possible. If we intend to widely scan those parameters or would like to include more than a single mode, it becomes, however, practically unfeasible. A (self-consistent) perturbative correction[84,85,89] to the electronic quantities might suffice to suppress some of the problematic features. Such a correction could be constructed via static electronic polarizabilities, which can be predicted with an additional neural network,[79] to correct the electronic energies and dipole moments according to the adiabatic cavity field. We envision to combine such a corrected treatment with a full graphical processor unit (GPU) implementation of our approach, which would dramatically reduce the required computational time and pave the way toward explicit ensembles, solvents, and accurate estimates of the chemical kinetics.

◼ CONCLUSIONS

Recent years have seen a rapid development of theoretical models for the description of strong light−matter coupling and polaritonic chemistry in particular. Most theoretical work focuses on model systems, which is natural given the young age of the field, and yet this poses a major challenge as overly simplified models are unable to truly connect to experiment. Here, we illustrate a combination of *ab initio* trained ML models and modular cavity MD that aims to describe realistic molecules in realistic optical environments. This work allows, for the first time, the direct correlation of theoretical predictions to the experimentally measured changes in chemical kinetics.

We describe theoretically the appearance of single-molecule strong coupling and its influence on the Si−C bond for the experimentally investigated S_N2 reaction.[14] A clear frequency dependence of the rate constant, a critical aspect of polaritonic chemistry, is observed and translates into changes in enthalpy and entropy that are consistent with the experimental observations. Interestingly, we observe inhibiting and *catalyzing* effects for the same reaction, the latter of which stand in contrast to previous *ab initio* calculations.[13] In total, three different regimes can be identified that are set apart by

differences in the kinetic changes. (i) A strongly inhibiting effect without a clear vibrational contribution results in a strong increase in enthalpy but relatively small increase in entropy. (ii) Vibrationally supported catalysis predominantly increases the entropy and only slightly lowers the enthalpy, which results effectively in a simple shift in the Eyring plot, but we emphasize that the shorter reaction time likely results in an overestimation of this effect. (iii) Vibrationally supported inhibition raises the enthalpy and results in the strongest increase in entropy. The latter observation is qualitatively consistent with experiment and suggests a slight change in the chemical character of the reaction. Vibrationally supported rate changes (ii, iii) are accompanied by a more pronounced change in the normal-mode occupation in optically active domains, suggesting that the microscopic mechanism is caused by a stronger interplay of optically active modes via the cavity, i.e., by cavity mediated changes in the redistribution of vibrational energy.

The discrepancy with *ab initio* calculations, although sharing comparable patterns when scanning the cavity frequency and comparing identical ensembles, suggests that dynamic changes in electronic polarization induced by nuclear motion and mediated by the cavity play a considerable role at the selected coupling strength. This might explain why many simplified MD simulations aiming to understand vibrational strong coupling have been able to capture some frequency dependence but often showed strong detuning, or simultaneous catalyzing and inhibiting features for the same reaction, which, to the best of our knowledge, is in conflict with current experimental work. Our work demonstrates therefore the importance of *ab initio* QED in the future of polaritonic chemistry and emphasizes the significance of theory that is tailored to describe experimentally relevant reactions. Future development will focus on (self-consistent) perturbative corrections and the full transfer of the established framework to GPUs, thus providing access to realistic (optical) environments and an explicit description of solute−solvent ensembles. The latter is essential for investigating potential modification of solvation dynamics induced by strong coupling.[18,88,90]

Polaritonic chemistry remains an equally fascinating and puzzling domain of research. While major questions are yet to be answered,[2−4,6] especially the connection between local chemistry and collective coupling as well as the interplay with solvation, the continuous growth of theoretical methodology and additional experiments draw an optimistic picture for the future of polaritonics. Our work adds to this a new facet and a clear perspective for possible future development, providing a valuable insight that can be experimentally validated.

ASSOCIATED CONTENT

Data Availability Statement

Training data, inputs, and final NEP models are available via Zenodo 10.5281/zenodo.10255268.

Ⓢ Supporting Information

The Supporting Information is available free of charge at https://pubs.acs.org/doi/10.1021/jacs.3c12829.

> Information on the training procedure and performance estimates for the NEP models, numerical and simulation details, derivation and implementation of optical forces, *NVT* calculations with corresponding estimates for enthalpy and entropy, details for kinetic estimates from *NVE* calculations (including Arrhenius plots), details

and results for rate and Si−C distance estimates for consistency check, details for normal-mode projections and Si−C stretching contributions, units, second evaluation of the consistency check based on a different NEP model trained from DFT calculations using the smaller 6-31G* basis, and extensive information and data on the calculation of vibrational frequencies (intermediate and transition states) (PDF)

AUTHOR INFORMATION

Corresponding Authors

Christian Schäfer − *Department of Physics, Chalmers University of Technology, 412 96 Göteborg, Sweden; Department of Microtechnology and Nanoscience, MC2, Chalmers University of Technology, 412 96 Göteborg, Sweden;* ⓞ orcid.org/0000-0002-8557-733X; Email: christian.schaefer.physics@gmail.com

Paul Erhart − *Department of Physics, Chalmers University of Technology, 412 96 Göteborg, Sweden;* ⓞ orcid.org/0000-0002-2516-6061; Email: erhart@chalmers.se

Authors

Jakub Fojt − *Department of Physics, Chalmers University of Technology, 412 96 Göteborg, Sweden*

Eric Lindgren − *Department of Physics, Chalmers University of Technology, 412 96 Göteborg, Sweden;* ⓞ orcid.org/0000-0002-8549-6839

Complete contact information is available at: https://pubs.acs.org/10.1021/jacs.3c12829

Notes

The authors declare no competing financial interest.

ADDITIONAL NOTE

[a]Note in Figure 3 of ref 87 the $\propto 1/\omega$ decay for fixed V_c, i.e., with fixed g_0/ω_c, one would obtain $g_0^2/\omega_c = g_0^2/\omega_c^2 \omega_c \propto \omega_c$.

■ REFERENCES

(1) Genet, C.; Faist, J.; Ebbesen, T. W. Inducing new material properties with hybrid light−matter states. *Phys. Today* **2021**, *74*, 42−48.

(2) Garcia-Vidal, F. J.; Ciuti, C.; Ebbesen, T. W. Manipulating matter by strong coupling to vacuum fields. *Science* **2021**, *373*, No. eabd0336.

(3) Simpkins, B. S.; Dunkelberger, A. D.; Owrutsky, J. C. Mode-specific chemistry through vibrational strong coupling (or A wish come true). *J. Phys. Chem. C* **2021**, *125*, 19081−19087.

(4) Sidler, D.; Ruggenthaler, M.; Schäfer, C.; Ronca, E.; Rubio, A. A perspective on *ab initio* modeling of polaritonic chemistry: the role of non-equilibrium effects and quantum collectivity. *J. Chem. Phys.* **2022**, *156*, 230901.

(5) Ruggenthaler, M.; Sidler, D.; Rubio, A. Understanding polaritonic chemistry from *ab initio* quantum electrodynamics. *Chem. Rev.* **2023**, *123*, 11191−11229.

(6) Mandal, A.; Taylor, M. A.; Weight, B. M.; Koessler, E. R.; Li, X.; Huo, P. Theoretical advances in polariton chemistry and molecular cavity quantum electrodynamics. *Chem. Rev.* **2023**, *123*, 9786−9879.

(7) Hutchison, J. A.; Schwartz, T.; Genet, C.; Devaux, E.; Ebbesen, T. W. Modifying chemical landscapes by coupling to vacuum fields. *Angew. Chem., Int. Ed.* **2012**, *51*, 1592−1596.

(8) Munkhbat, B.; Wersäll, M.; Baranov, D. G.; Antosiewicz, T. J.; Shegai, T. Suppression of photo-oxidation of organic chromophores by strong coupling to plasmonic nanoantennas. *Sci. Adv.* **2018**, *4*, No. eaas9552.

(9) Ahn, W.; Triana, J. F.; Recabal, F.; Herrera, F.; Simpkins, B. S. Modification of ground-state chemical reactivity via light−matter coherence in infrared cavities. *Science* **2023**, *380*, 1165−1168.

(10) Chen, T.-T.; Du, M.; Yang, Z.; Yuen-Zhou, J.; Xiong, W. Cavity-enabled enhancement of ultrafast intramolecular vibrational redistribution over pseudorotation. *Science* **2022**, *378*, 790−794.

(11) Galego, J.; Garcia-Vidal, F. J.; Feist, J. Suppressing photo-chemical reactions with quantized light fields. *Nat. Commun.* **2016**, *7*, 13841.

(12) Fregoni, J.; Granucci, G.; Persico, M.; Corni, S. Strong coupling with light enhances the photoisomerization quantum yield of azobenzene. *Chem* **2020**, *6*, 250−265.

(13) Schäfer, C.; Flick, J.; Ronca, E.; Narang, P.; Rubio, A. Shining light on the microscopic resonant mechanism responsible for cavity-mediated chemical reactivity. *Nat. Commun.* **2022**, *13*, 7817.

(14) Thomas, A.; George, J.; Shalabney, A.; Dryzhakov, M.; Varma, S. J.; Moran, J.; Chervy, T.; Zhong, X.; Devaux, E.; Genet, C.; Hutchison, J. A.; Ebbesen, T. W. Ground-state chemical reactivity under vibrational coupling to the vacuum electromagnetic field. *Angew. Chem., Int. Ed.* **2016**, *55*, 11462−11466.

(15) Thomas, A.; Jayachandran, A.; Lethuillier-Karl, L.; Vergauwe, R. M.; Nagarajan, K.; Devaux, E.; Genet, C.; Moran, J.; Ebbesen, T. W. Ground state chemistry under vibrational strong coupling: dependence of thermodynamic parameters on the Rabi splitting energy. *Nanophotonics* **2020**, *9*, 249−255.

(16) Gu, K.; Si, Q.; Li, N.; Gao, F.; Wang, L.; Zhang, F. Regulation of recombinase polymerase amplification by vibrational strong coupling of water. *ACS Photonics* **2023**, *10*, 1633−1637.

(17) Thomas, A.; Lethuillier-Karl, L.; Nagarajan, K.; Vergauwe, R. M. A.; George, J.; Chervy, T.; Shalabney, A.; Devaux, E.; Genet, C.; Moran, J.; Ebbesen, T. W. Tilting a ground-state reactivity landscape by vibrational strong coupling. *Science* **2019**, *363*, 615−619.

(18) Singh, J.; Lather, J.; George, J. Solvent dependence on cooperative vibrational strong coupling and cavity catalysis. *ChemPhysChem* **2023**, *24*, No. e202300016.

(19) Wiesehan, G. D.; Xiong, W. Negligible rate enhancement from reported cooperative vibrational strong coupling catalysis. *J. Chem. Phys.* **2021**, *155*, 241103.

(20) Schäfer, C.; Ruggenthaler, M.; Rubio, A. *Ab initio* nonrelativistic quantum electrodynamics: bridging quantum chemistry and quantum optics from weak to strong coupling. *Phys. Rev. A* **2018**, *98*, 043801.

(21) Chikkaraddy, R.; de Nijs, B.; Benz, F.; Barrow, S. J.; Scherman, O. A.; Rosta, E.; Demetriadou, A.; Fox, P.; Hess, O.; Baumberg, J. J. Single-molecule strong coupling at room temperature in plasmonic nanocavities. *Nature* **2016**, *535*, 127−130.

(22) Wang, D.; Kelkar, H.; Martin-Cano, D.; Utikal, T.; Götzinger, S.; Sandoghdar, V. Coherent coupling of a single molecule to a scanning Fabry-Perot microcavity. *Phys. Rev. X* **2017**, *7*, 021014.

(23) Ojambati, O. S.; Chikkaraddy, R.; Deacon, W. D.; Horton, M.; Kos, D.; Turek, V. A.; Keyser, U. F.; Baumberg, J. J. Quantum electrodynamics at room temperature coupling a single vibrating molecule with a plasmonic nanocavity. *Nat. Commun.* **2019**, *10*, 1049.

(24) Flick, J.; Ruggenthaler, M.; Appel, H.; Rubio, A. Atoms and molecules in cavities, from weak to strong coupling in quantum-electrodynamics (QED) chemistry. *Proc. Natl. Acad. Sci. U.S.A.* **2017**, *114*, 3026−3034.

(25) Haugland, T. S.; Ronca, E.; Kjønstad, E. F.; Rubio, A.; Koch, H. Coupled cluster theory for molecular polaritons: changing ground and excited states. *Phys. Rev. X* **2020**, *10*, 041043.

(26) Arul, R.; Grys, D.-B.; Chikkaraddy, R.; Mueller, N. S.; Xomalis, A.; Miele, E.; Euser, T. G.; Baumberg, J. J. Giant mid-IR resonant coupling to molecular vibrations in sub-nm gaps of plasmonic multilayer metafilms. *Light: Sci. Appl.* **2022**, *11*, 281.

(27) Coles, D. M.; Somaschi, N.; Michetti, P.; Clark, C.; Lagoudakis, P. G.; Savvidis, P. G.; Lidzey, D. G. Polariton-mediated energy transfer between organic dyes in a strongly coupled optical microcavity. *Nat. Mater.* **2014**, *13*, 712−719.

(28) Orgiu, E.; George, J.; Hutchison, J. A.; Devaux, E.; Dayen, J. F.; Doudin, B.; Stellacci, F.; Genet, C.; Schachenmayer, J.; Genes, C.; Pupillo, G.; Samorì, P.; Ebbesen, T. W. Conductivity in organic semiconductors hybridized with the vacuum field. *Nat. Mater.* **2015**, *14*, 1123−1129.

(29) Zhong, X.; Chervy, T.; Wang, S.; George, J.; Thomas, A.; Hutchison, J. A.; Devaux, E.; Genet, C.; Ebbesen, T. W. Non-radiative energy transfer mediated by hybrid light-matter states. *Angew. Chem., Int. Ed.* **2016**, *55*, 6202−6206.

(30) Fukushima, T.; Yoshimitsu, S.; Murakoshi, K. Inherent promotion of ionic conductivity via collective vibrational strong coupling of water with the vacuum electromagnetic field. *J. Am. Chem. Soc.* **2022**, *144*, 12177−12183.

(31) Wellnitz, D.; Pupillo, G.; Schachenmayer, J. Disorder enhanced vibrational entanglement and dynamics in polaritonic chemistry. *Commun. Phys.* **2022**, *5*, 120.

(32) Herrera, F.; Spano, F. C. Cavity-controlled chemistry in molecular ensembles. *Phys. Rev. Lett.* **2016**, *116*, 238301.

(33) Schäfer, C.; Ruggenthaler, M.; Appel, H.; Rubio, A. Modification of excitation and charge transfer in cavity quantum-electrodynamical chemistry. *Proc. Natl. Acad. Sci. U.S.A.* **2019**, *116*, 4883−4892.

(34) Groenhof, G.; Climent, C.; Feist, J.; Morozov, D.; Toppari, J. J. Tracking polariton relaxation with multiscale molecular dynamics simulations. *J. Phys. Chem. Lett.* **2019**, *10*, 5476−5483.

(35) Csehi, A.; Vendrell, O.; Halász, G. J.; Vibók, Á. Competition between collective and individual conical intersection dynamics in an optical cavity. *New J. Phys.* **2022**, *24*, 073022.

(36) Campos-Gonzalez-Angulo, J. A.; Ribeiro, R. F.; Yuen-Zhou, J. Resonant catalysis of thermally activated chemical reactions with vibrational polaritons. *Nat. Commun.* **2019**, *10*, 4685.

(37) Li, T. E.; Nitzan, A.; Subotnik, J. E. Collective vibrational strong coupling effects on molecular vibrational relaxation and energy transfer: numerical insights via cavity molecular dynamics simulations. *Angew. Chem., Int. Ed.* **2021**, *60*, 15533−15540.

(38) Kumar, S.; Biswas, S.; Rashid, U.; Mony, K. S.; Vergauwe, R.; Kaliginedi, V.; Thomas, A. Extraordinary electrical conductance of non-conducting polymers under vibrational strong coupling. *arXiv* **2023**, arXiv:2303.03777.

(39) Stumper, S.; Okamoto, J. Localization and spectrum of quasiparticles in a disordered fermionic Dicke model. *Phys. Rev. B* **2023**, *108*, 184206.

(40) Bhatt, P.; Dutta, J.; Kaur, K.; George, J. Long-range energy transfer in strongly coupled donor−acceptor phototransistors. *Nano Lett.* **2023**, *23*, 5004−5011.

(41) Timmer, D.; Gittinger, M.; Quenzel, T.; Stephan, S.; Zhang, Y.; Schumacher, M. F.; Lützen, A.; Silies, M.; Tretiak, S.; Zhong, J. H.; et al. Plasmon mediated coherent population oscillations in molecular aggregates. *Nat. Commun.* **2023**, *14*, 8035.

(42) Cui, B.; Sukharev, M.; Nitzan, A. Comparing semiclassical mean-field and 1-exciton approximations in evaluating optical response under strong light−matter coupling conditions. *J. Chem. Phys.* **2023**, *158*, 164113.

(43) Engelhardt, G.; Cao, J. Polariton localization and dispersion properties of disordered quantum emitters in multimode microcavities. *Phys. Rev. Lett.* **2023**, *130*, 213602.

(44) Peter, E.; Senellart, P.; Martrou, D.; Lemaître, A.; Hours, J.; Gérard, J. M.; Bloch, J. Exciton-photon strong-coupling regime for a single quantum dot embedded in a microcavity. *Phys. Rev. Lett.* **2005**, *95*, 067401.

(45) Liu, X.; Galfsky, T.; Sun, Z.; Xia, F.; Lin, E.-c.; Lee, Y.-H.; Kéna-Cohen, S.; Menon, V. M. Strong light−matter coupling in two-dimensional atomic crystals. *Nat. Photonics* **2015**, *9*, 30−34.

(46) Jarc, G.; Mathengattil, S. Y.; Montanaro, A.; Giusti, F.; Rigoni, E. M.; Sergo, R.; Fassioli, F.; Winnerl, S.; Dal Zilio, S.; Mihailovic, D.; et al. Cavity-mediated thermal control of metal-to-insulator transition in 1T-TaS2. *Nature* **2023**, *622*, 487−492.

(47) Latini, S.; Shin, D.; Sato, S. A.; Schäfer, C.; De Giovannini, U.; Hübener, H.; Rubio, A. The ferroelectric photo ground state of SrTiO$_3$: cavity materials engineering. *Proc. Natl. Acad. Sci. U.S.A.* **2021**, *118*, No. e2105618118.

(48) Lenk, K.; Li, J.; Werner, P.; Eckstein, M. Dynamical mean-field study of a photon-mediated ferroelectric phase transition. *Phys. Rev. B* **2022**, *106*, 245124.

(49) Galego, J.; Climent, C.; Garcia-Vidal, F. J.; Feist, J. Cavity Casimir-Polder forces and their effects in ground-state chemical reactivity. *Phys. Rev. X* **2019**, *9*, 021057.

(50) Campos-Gonzalez-Angulo, J. A.; Yuen-Zhou, J. Polaritonic normal modes in transition state theory. *J. Chem. Phys.* **2020**, *152*, 161101.

(51) Li, T. E.; Nitzan, A.; Subotnik, J. E. On the origin of ground-state vacuum-field catalysis: equilibrium consideration. *J. Chem. Phys.* **2020**, *152*, 234107.

(52) Li, X.; Mandal, A.; Huo, P. Cavity frequency-dependent theory for vibrational polariton chemistry. *Nat. Commun.* **2021**, *12*, 1315.

(53) Sun, J.; Vendrell, O. Suppression and enhancement of thermal chemical rates in a cavity. *J. Phys. Chem. Lett.* **2022**, *13*, 4441−4446.

(54) Sun, J.; Vendrell, O. Modification of thermal chemical rates in a cavity via resonant effects in the collective regime. *J. Phys. Chem. Lett.* **2023**, *14*, 8397−8404.

(55) Lindoy, L. P.; Mandal, A.; Reichman, D. R. Resonant cavity modification of ground-state chemical kinetics. *J. Phys. Chem. Lett.* **2022**, *13*, 6580−6586.

(56) Ruggenthaler, M.; Flick, J.; Pellegrini, C.; Appel, H.; Tokatly, I. V.; Rubio, A. Quantum-electrodynamical density-functional theory: bridging quantum optics and electronic-structure theory. *Phys. Rev. A* **2014**, *90*, 012508.

(57) Tokatly, I. V. Time-dependent density functional theory for many-electron systems interacting with cavity photons. *Phys. Rev. Lett.* **2013**, *110*, 233001.

(58) Flick, J.; Narang, P. Cavity-correlated electron-nuclear dynamics from first principles. *Phys. Rev. Lett.* **2018**, *121*, 113002.

(59) Schäfer, C.; Buchholz, F.; Penz, M.; Ruggenthaler, M.; Rubio, A. Making *ab initio* QED functional (s): nonperturbative and photon-free effective frameworks for strong light−matter coupling. *Proc. Natl. Acad. Sci. U.S.A.* **2021**, *118*, No. e2110464118.

(60) Loudon, R. *The Quantum Theory of Light*; Oxford Science Publications, 1988.

(61) Craig, D.; Thirunamachandran, T.. In *Molecular Quantum Electrodynamics: An Introduction to Radiation-Molecule Interactions*; *Dover Books on Chemistry Series*; Dover Publications, 1998.

(62) Schäfer, C.; Ruggenthaler, M.; Rokaj, V.; Rubio, A. Relevance of the quadratic diamagnetic and self-polarization terms in cavity quantum electrodynamics. *ACS Photonics* **2020**, *7*, 975−990.

(63) Buhmann, S. Y. *Dispersion Forces I: Macroscopic Quantum Electrodynamics and Ground-State Casimir, Casimir−Polder and van der Waals Forces*; Springer, 2013; Vol. 247.

(64) Lentrodt, D.; Evers, J. *Ab initio* few-mode theory for quantum potential scattering problems. *Phys. Rev. X* **2020**, *10*, 011008.

(65) Feist, J.; Fernández-Domínguez, A. I.; García-Vidal, F. J. Macroscopic QED for quantum nanophotonics: emitter-centered modes as a minimal basis for multiemitter problems. *Nanophotonics* **2020**, *10*, 477−489.

(66) Schäfer, C.; Johansson, G. Shortcut to self-consistent light-matter interaction and realistic spectra from first principles. *Phys. Rev. Lett.* **2022**, *128*, 156402.

(67) Schäfer, C. Polaritonic chemistry from first principles via embedding radiation reaction. *J. Phys. Chem. Lett.* **2022**, *13*, 6905−6911.

(68) Li, T. E.; Subotnik, J. E.; Nitzan, A. Cavity molecular dynamics simulations of liquid water under vibrational ultrastrong coupling. *Proc. Natl. Acad. Sci. U.S.A.* **2020**, *117*, 18324−18331.

(69) Sidler, D.; Schäfer, C.; Ruggenthaler, M.; Rubio, A. Polaritonic Chemistry: collective strong coupling implies strong local modification of chemical properties. *J. Phys. Chem. Lett.* **2021**, *12*, 508−516.

(70) Sidler, D.; Schnappinger, T.; Obzhirov, A.; Ruggenthaler, M.; Kowalewski, M.; Rubio, A. Unraveling a cavity induced molecular polarization mechanism from collective vibrational strong coupling. *arXiv* **2023**, arXiv:2306.06004.

(71) Schnappinger, T.; Sidler, D.; Ruggenthaler, M.; Rubio, A.; Kowalewski, M. Cavity Born−Oppenheimer Hartree−Fock ansatz: light−matter properties of strongly coupled molecular ensembles. *J. Phys. Chem. Lett.* **2023**, *14*, 8024−8033.

(72) Hjorth Larsen, A.; Jørgen Mortensen, J.; Blomqvist, J.; Castelli, I. E.; Christensen, R.; Dułak, M.; Friis, J.; Groves, M. N.; Hammer, B.; Hargus, C.; et al. The atomic simulation environment—a Python library for working with atoms. *J. Phys.: Condens. Matter* **2017**, *29*, 273002.

(73) Marx, D.; Hutter, J. *Ab Initio Molecular Dynamics: Basic Theory and Advanced Methods*; Cambridge University Press, 2009.

(74) Van Beest, B.; Kramer, G. J.; Van Santen, R. Force fields for silicas and aluminophosphates based on *ab initio* calculations. *Phys. Rev. Lett.* **1990**, *64*, 1955−1958.

(75) Ponder, J. W.; Case, D. A. Force fields for protein simulations. *Adv. Protein Chem.* **2003**, *66*, 27−85.

(76) Fan, Z.; Zeng, Z.; Zhang, C.; Wang, Y.; Song, K.; Dong, H.; Chen, Y.; Ala-Nissila, T. Neuroevolution machine learning potentials: combining high accuracy and low cost in atomistic simulations and application to heat transport. *Phys. Rev. B* **2021**, *104*, 104309.

(77) Fan, Z. Improving the accuracy of the neuroevolution machine learning potential for multi-component systems. *J. Phys.: Condens. Matter* **2022**, *34*, 125902.

(78) Fan, Z.; Wang, Y.; Ying, P.; Song, K.; Wang, J.; Wang, Y.; Zeng, Z.; Xu, K.; Lindgren, E.; Rahm, J. M.; et al. GPUMD: a package for constructing accurate machine-learned potentials and performing highly efficient atomistic simulations. *J. Chem. Phys.* **2022**, *157*, 114801.

(79) Xu, N.; Rosander, P.; Schäfer, C.; Lindgren, E.; Österbacka, N.; Fang, M.; Chen, W.; He, Y.; Fan, Z.; Erhart, P. Tensorial properties via the neuroevolution potential framework: fast simulation of infrared and Raman spectra. *arXiv* **2023**, arXiv:2312.05233.

(80) Li, X.; Mandal, A.; Huo, P. Theory of mode-selective chemistry through polaritonic vibrational strong coupling. *J. Phys. Chem. Lett.* **2021**, *12*, 6974−6982.

(81) Lindoy, L. P.; Mandal, A.; Reichman, D. R. Quantum dynamical effects of vibrational strong coupling in chemical reactivity. *Nat. Commun.* **2023**, *14*, 2733.

(82) Fiechter, M. R.; Runeson, J. E.; Lawrence, J. E.; Richardson, J. O. How quantum is the resonance behavior in vibrational polariton chemistry? *J. Phys. Chem. Lett.* **2023**, *14* (36), 8261−8267.

(83) Flick, J.; Appel, H.; Ruggenthaler, M.; Rubio, A. Cavity Born-Oppenheimer approximation for correlated electron-nuclear-photon systems. *J. Chem. Theory Comput.* **2017**, *13*, 1616−1625.

(84) Bonini, J.; Flick, J. *Ab initio* linear-response approach to vibro-polaritons in the cavity Born−Oppenheimer approximation. *J. Chem. Theory Comput.* **2022**, *18*, 2764−2773.

(85) Fischer, E. W.; Saalfrank, P. Beyond cavity Born−Oppenheimer: on nonadiabatic coupling and effective ground state Hamiltonians in vibro-polaritonic chemistry. *J. Chem. Theory Comput.* **2023**, *19*, 7215−7229.

(86) Pellegrini, C.; Flick, J.; Tokatly, I. V.; Appel, H.; Rubio, A. Optimized effective potential for quantum electrodynamical time-dependent density functional theory. *Phys. Rev. Lett.* **2015**, *115*, 093001.

(87) Riso, R. R.; Haugland, T. S.; Ronca, E.; Koch, H. Molecular orbital theory in cavity QED environments. *Nat. Commun.* **2022**, *13*, 1368.

(88) Piejko, M.; Patrahau, B.; Joseph, K.; Muller, C.; Devaux, E.; Ebbesen, T. W.; Moran, J. Solvent polarity under vibrational strong coupling. *J. Am. Chem. Soc.* **2023**, *145*, 13215−13222.

(89) Szidarovszky, T. An efficient and flexible approach for computing rovibrational polaritons from first principles. *J. Chem. Phys.* **2023**, *159*, 014112.

(90) Castagnola, M.; Haugland, T. S.; Ronca, E.; Koch, H.; Schäfer, C. Collective strong coupling modifies aggregation and solvation. *J. Phys. Chem. Lett.* **2024**, *15*, 1428−1434.